



## A comparative study on physicochemical properties and photocatalytic behavior of two different nanostructure composite TiO<sub>2</sub> films coated on glass substrate

Mojtaba Nasr-Esfahani<sup>a\*</sup>, Mohammad Hossein Habibi<sup>b</sup>

<sup>a</sup>Department of Materials Science and Engineering, Islamic Azad University, Najafabad Branch, Iran

Tel./Fax: +98 311 253 6771; email: m-nasresfahani@iaun.ac.ir, mnstd@sci.ui.ac.ir

<sup>b</sup>Department of Chemistry, University of Isfahan, Isfahan, 81746-73441, Iran

Received 30 April 2008; Accepted 27 January 2009

### ABSTRACT

Two types of composite films (MPC500SGF-MC and ANPSGF-MC) have been synthesized by a modified sol-gel method using different particle sizes of TiO<sub>2</sub> powder. Methyl cellulose was added as a template to the sol for stress reduction which improved not only the amount of crystalline material immobilized on the support, but also the nanosize of the films calcined at 500°C. The physicochemical properties, including surface morphology, crystal size and adhesion on the glass substrate, were investigated by SEM and XRD. The photocatalytic activities of the films were compared using methyl orange (MO) as a model organic contaminant in water. The results on photocatalytic degradation of MO showed that the increase in photocatalytic activity for Aldrich TiO<sub>2</sub> powder (ANP) calcined at 500°C, compared with that of Millennium PC500 composite film. The optimum degradation conditions of MO solution are determined. This study proves that particle size of starting TiO<sub>2</sub> material is important for the preparation of nanostructured TiO<sub>2</sub> composite film with enhanced photocatalytic activity and excellent adhesion on the glass substrate.

**Keywords:** Millennium PC500; Aldrich TiO<sub>2</sub> powder; Sol-gel; Methyl orange; Nanostructure; Composite film; Methyl cellulose; Coated on glass

### 1. Introduction

The use of semiconductor oxides particles as photocatalysts is well established and has shown great utility in the complete mineralization of organic pollutants. Among these semiconductors, nanosized TiO<sub>2</sub> has been proved to be an excellent catalyst in the photocatalytic degradation of organic pollutants because it is an effective, photo-stable, reusable, inexpensive, non-toxic and easily available catalyst [1]. However, it is evident that in any wastewater purification process, filtration and resuspension of semiconductor powder should be avoided if possible.

The above problems can be eliminated by immobilizing a TiO<sub>2</sub> catalyst over suitable supports. Different forms of TiO<sub>2</sub>, such as thin and thick film coatings, have been utilized to make this catalyst more efficient and more applicable. TiO<sub>2</sub> thin films are synthesized by a variety of methods like sol-gel [2,3], chemical vapor deposition (CVD) [4], electrodeposition and electrophoresis. Several research groups have reported the use of TiO<sub>2</sub> thin film in photocatalytic degradation of organic impurities in water [5–7]. However, the relatively low surface area of the deposited layer effectively limits the photo-efficiency of such thin coatings. As a result, these kinds of titanium dioxide coatings have not been considered as good candidates for large-scale applications such as purification of water or air.

\*Corresponding author.

Nanostructured ceramic oxide films and coatings can be deposited using sol–gel type methods [8,9]. Sol–gel processing is especially adaptable for film formation. Films and coatings represent the earliest commercial use of sol–gel processing. Sol–gel techniques offer the following advantages in coatings: control of microstructure, pore size, and surface area. By controlling these parameters, the film properties can be tailored. Dense pinhole-free layers can be prepared at low temperatures using sol–gel processing. Sol–gel films can be deposited by spraying, dip coating, and spin coating. Because the large capillary stress during solvent evaporation can cause cracking, the sol–gel process has been traditionally used for preparing thin films and coatings. To prepare thick coatings, the problems of shrinkage and cracking and the limitation of coating thickness can be mitigated by increasing particle loading in the sol–gel process [10]. This approach involved dispersing large ceramic powders in sol–gel solution, and applying the mixture onto the substrate by various techniques such as dipping and spraying. Coatings with thicknesses up to 200  $\mu\text{m}$  were fabricated. The sol–gel film formed strong bonds to both oxide powders and substrates by interaction with functionalized surface hydroxyl groups on the oxide powders and the oxide layer of substrates and strong bond reduced cracking. The shrinkage problem associated with the conventional sol–gel approach was minimized due to the high loading of ceramic powders.

Because of sol–gel-processed inorganic–organic composite materials are attractive and capable of producing not only sufficiently thick films by single coating without cracking, but also producing films with novel properties. We explored in our previous study [11] another approach to achieve useful materials for photocatalytic application by direct mixing of dispersed  $\text{TiO}_2$  titanium dioxide in sol–gel solution with prepolymerized material (polymer). The polymer was introduced into the sol–gel precursors in order to prevent particle aggregation, adjust the viscosity of sol, increase the strength of the unfired materials, and prevent film crack formation. In this case, it is important to avoid phase separation throughout the sol–gel reaction by a careful choice of solvents and optimized material-processing conditions. Methyl cellulose (MC) is one of the ideal pre-polymerized materials due to its solubility in water, which is suitable for use in sol–gel processing. Another advantage is that MC belongs to non-ionic cellulose ether, which is substantially free of substances that can induce crystallization of silica or titania, etc. during any of the coating formation and densification process steps.

In this study the effect of  $\text{TiO}_2$  particle size on physicochemical properties and photocatalytic behavior of two different nanostructure composite  $\text{TiO}_2$  films coated on glass substrate is investigated. The various

factors such as time, concentration, pH and  $\text{H}_2\text{O}_2$  concentration were studied on photodegradation of MO in the presence of nanostructure composite films.

## 2. Experimental

### 2.1. Catalysts preparation

#### 2.1.1. Materials

A standard ethanol solution ( $M = 46.07 \text{ g/mol}$ , purity  $\approx 99.8\%$ ) was purchased from Fluka Chemical. Hydrochloric acid ( $M = 36.5 \text{ g/mol}$ , purity  $\approx 35.5\%$ ) was supplied from Merck. Titanium tetra isopropoxide [ $\text{Ti}(\text{OPr})_4$  or TITP] (Aldrich, 97%), the precursor, was used without further purification. Two types of commercial  $\text{TiO}_2$  powders, namely Aldrich  $\text{TiO}_2$  powder (ANP) and Millennium PC-500 (MPC500), were used as the filler in the nanostructure composite films. Specifications of the photocatalyst filler according to the manufacturer's data are given in Table 1. MC (low substitution) was obtained from Harris Chemical and used as an organic binder material. MO (4-[[4-dimethylamino]phenyl]azo) benzenesulfonic acid sodium salt) analytical grade (100% purity) provided from Aldrich was chosen as a simple model of a series of common azo-dyes largely used in the industry. Methyl Orange (MO) is a well known acid–base indicator, which is orange in a basic medium and red in an acidic medium. Its structure, reported in Fig. 1, is characterized by sulphonic groups, which are responsible for the high solubility of these dyes in water.

#### 2.1.2. Composite films preparation

The preparation steps for the composite films derived from  $\text{TiO}_2$  powder are described detail elsewhere [11]. The sol solution was prepared by adding 5ml TTP to a 50ml beaker containing a mixture of 10ml ethanol and 1.8ml

Table 1  
Properties of  $\text{TiO}_2$  nanopowders

Photocatalyst	Composition	Specific BET surface area ( $\text{m}^2\text{g}^{-1}$ )	Primary particle size (nm)
Aldrich $\text{TiO}_2$ powder,	$\geq 97\%$ anatase	190–290	15
Millennium PC-500	$\geq 97\%$ anatase	>250	5–10

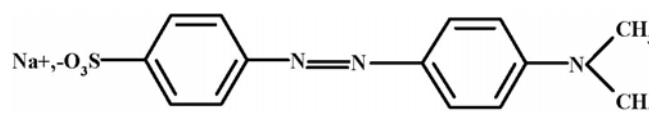


Fig. 1. Chemical structure of MO.

HCl 35.5% that had been mixed for 5 min. The mixture was vigorously stirred during addition and for a further 120 min after addition of the precursor at room temperature. MC 2 wt.% solution was prepared using MC and double-distilled water. These two solutions (titanium precursor and MC solution) were added dropwise and stirred overnight at room temperature. The molar ratio was TTP:HCl:EtOH:H<sub>2</sub>O, 1:1.1:10:10. Precalcined TiO<sub>2</sub> nanopowders were used as filler mixed with the sol (5% of sol). TiO<sub>2</sub> powder was dispersed in the sol and the prepared mixtures were deposited on the microscope glass slide (75 mm×25 mm×1 mm) by home made spin coating. The dried films were heated in a muffle furnace to 500°C at a heating rate 5°C min<sup>-1</sup> and maintained at this temperature for 60 min and cooled at room temperature at a similar rate. These composite films were used for photocatalytic degradation; otherwise the photocatalysts were stored in the dark to avoid pre-activation by room light or sunlight.

## 2.2. Characterization of films

Film morphology was characterized by an environmental scanning electron microscope (ESEM, Jeol JSM-5300LV) with accelerating 10 kV. The phase composition of photocatalyst was studied by the powder and plate XRD technique. The X-ray diffraction patterns were obtained on a D8 Advanced Bruker X-ray diffractometer using Cu K $\alpha$  radiation at an angle of 2 $\theta$  from 15 to 60°. The scan speed was 0.03 2 $\theta$ .s<sup>-1</sup>. The strongest peaks of TiO<sub>2</sub> corresponding to anatase (1 0 1) were selected to evaluate the crystallinity of the samples. The mean crystallite size (L) was determined from the broadening  $\beta$  of the most intense line for each polymorph in the X-ray diffraction pattern based on the Scherer equation.

$$L = \frac{k\lambda}{\beta \cos\theta}$$

where  $\lambda$  is the radiation wavelength,  $k = 0.90$  and  $\theta$  the Bragg angle [12]. Evaluation of the adhesion and bonding strength between the coating and glass substrate was made by using the scratch test technique [13]. The mechanical integrity of coatings (deposited by spin coating method with the same controlled thickness) was measured using a motorised Clemen scratch tester (equipped with a tungsten carbide ball tool, 1 mm). Scratches were made under an applied load increasing from 0 to 1000 g, for the maximum length of 50 mm. The point of coating adhesive failure was determined by visual observation. The load at which the indenter started to scratch the substrate surface was considered as indicative of the coating resistance to scratch failure.

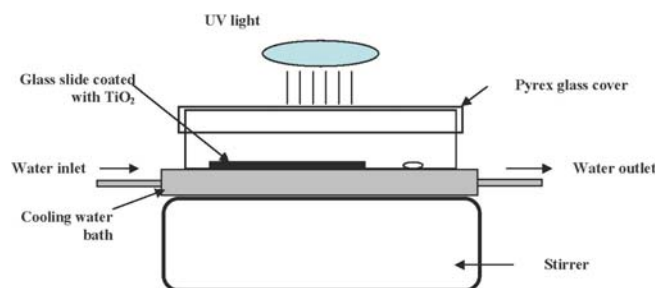


Fig. 2. Schematic diagram of the experimental set-up for photocatalytic reactions studies.

## 2.4. Photocatalytic experiments

Sol-gel derived composite films with Aldrich TiO<sub>2</sub> powder and Millennium PC-500 TiO<sub>2</sub> were prepared on microscopy glass slides. To evaluate the catalytic activity, the photodegradation of MO solution was chosen as a simple model of a series of common azo-dyes largely used in the industry. Experiments were performed at room temperature in a photoreactor measured by 40 cm × 15 cm × 15 cm (Fig. 2). One TiO<sub>2</sub>/glass with one time spin coating (75 mm × 25 mm × 1 mm) was used as photocatalyst and irradiated with two 8 W UV-A ( $\lambda = 365$  nm) at a distance of 5 cm from the top of the solutions. Ten ml of the dye solutions with an initial concentration of 5 ppm were used and oxygen was bubbled into each solution to ensure a saturation of oxygen before photoreaction. The solution was stirred in the dark for 90 min before irradiation to reach an equilibrated adsorption. Therefore, this time has been selected for the initial period to UV-irradiation to make sure that the initial degradation initiates at the equilibrium of the adsorption. In order to test the influence of pH on the adsorption and photoreactivity, some runs were carried out at different initial pHs: using NaOH or HCl (0.1 M) in which the absorption surface properties of TiO<sub>2</sub> are negligible [14]. Photocatalytic decomposition of MO was investigated at room temperature by varying the initial concentration of dye from 5 to 20 ppm under optimum conditions: pH=3.7; one glass slide coated composite film in 10 ml solution. The color removal of the dye solution was followed by measuring the absorbance value at  $\lambda=560$  nm, using a double-beam UV-visible spectrophotometer, (Varian, Cary 500 scan) initially calibrated according to Beer–Lambert's law.

## 3. Results and discussion

### 3.1. Properties of composite films

The XRD patterns of different sol-gel derived composite films with ANP and MPC500 compared with ANP and MPC500 powders are shown in Figs. 3 and 4,

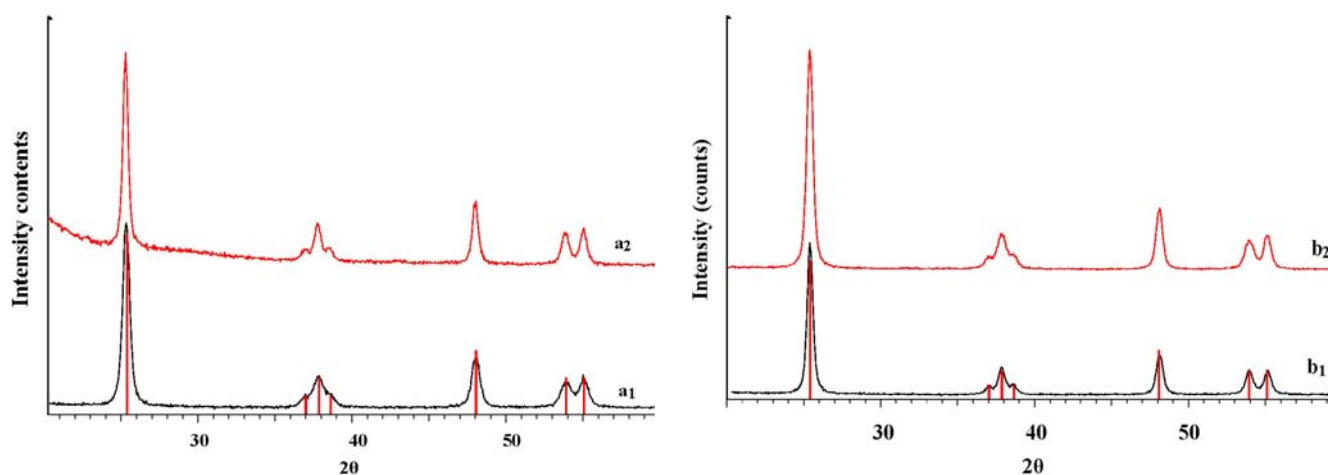


Fig. 3. X-ray diffraction patterns (a<sub>1</sub>) as-received Aldrich nanopowder TiO<sub>2</sub> (ANP) (a<sub>2</sub>) sol-gel derived composite film with Aldrich nanopowder TiO<sub>2</sub> (ANPSGF-MC) heat treated for 1 h at 500 °C, (b<sub>1</sub>) as-received Millennium PC-500 TiO<sub>2</sub> (MPC500) and (b<sub>2</sub>) sol-gel derived composite film with Millennium PC-500 TiO<sub>2</sub> (MPC500SGF-MC) heat treated for 1 h at 500 °C.

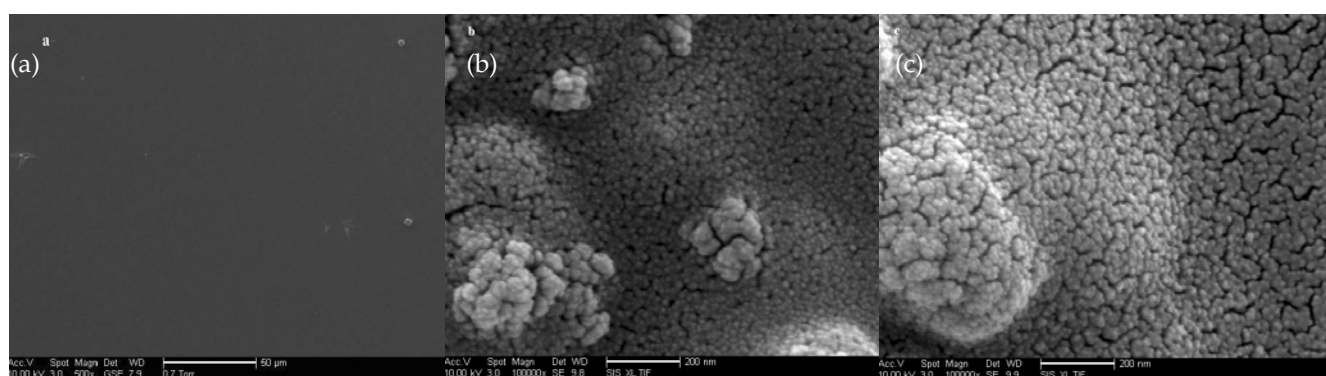


Fig. 4. Scanning electron micrographs of the surface of TiO<sub>2</sub> films made from the precursor sol containing (a) no nano-powder; (b) ANPSGF-MC and (c) MPC500SGF-MC. All the samples heat treated for 1 h at 500 °C.

respectively. It was shown previously [11] that the sol-gel-derived material, prior to the calcinations process, had an amorphous (and/or an ultra-fine crystalline) structure with a very broad peak at about  $2\theta=25^\circ$  (which is identified as the most intensive peak (101) for the anatase TiO<sub>2</sub>). As shown the anatase characteristic peaks became sharper in both composite films in compare with calcinated nanopowders which indicates that crystallite size of anatase phase increases markedly with calcination temperature (500 °C). The typical values of anatase crystallite size of sol-gel derived composite films and calcinated nonopowder were calculated by Scherrer's equation. As shown in Table 2, the size of the anatase crystallites in the composite films, both with ANP and MPC500, is increased with heat treatment, but the growth process of nanocrystalline anatase in composite film with MPC500 is more noticeable than other one. It is suggested that the growth process of nanocrystalline anatase is mainly because of sintering of the single crystals within agglomerates

and finally the original agglomerate transforms to a larger single crystal. Therefore, smaller particle size of MPC500 is considered as the main reason for the formation of larger particle size in corresponding composite film.

Surface morphology and thickness of one-dip-coating TiO<sub>2</sub> composite films prepared by ANP and MPC500 and calcined at 500 °C for 1 h were examined using ESEM analysis.

Figs. 4a–c show the morphology of TiO<sub>2</sub> composite films prepared at 0 and 5 wt.% ANP and MPC500 in the sol respectively. These ESEM images show that the surface of film prepared without nanopowder TiO<sub>2</sub> in the sol (plain sol, image a) is "smooth" without the presence of any visible agglomerates. On the other hand, the surfaces of films prepared with the nanopowders TiO<sub>2</sub> and the sol (images b and c) are full of visible agglomerates (a cluster of coagulated grains). In order to obtain more detailed information of the physical structure of these agglomerates

Table 2  
Physical and chemical characteristics of sol-gel derived composite films

Material	Heat treatment conditions	Particle size (nm) <sup>a</sup>	Average grain size (nm) <sup>b</sup>	Scratch adhesion (g/mm <sup>2</sup> )
ANPSGF-MC	—	14.9	—	9
	500°C, 1 h	16.3	19	200
MPC500SGF-MC	—	6.6	—	10
	500°C, 1 h	18.1	65	350

<sup>a</sup>Using Scherrer equation:  $D = 0.9\lambda / (B\cos\theta)$  where  $\lambda = 0.15418$  nm.

<sup>b</sup>Cluster of crystallites on the surface of the film in Fig. 4.

merates on the film surface, we performed ESEM analysis of the sol-gel derived composite films at 100,000 magnifications. As shown in Figs. 4b and c, the larger agglomerates are composed of many grains (i.e., clusters of crystallites consisting of crystallites from ANP and MPC500 particles and particles formed from alkoxide hydrolysis). Because all composite films are calcined at higher calcinations temperatures (500°C), the grains consisted of agglomerated secondary particles (i.e., sintered or aggregated crystallite mixtures from TIP hydrolysis and nanopowders TiO<sub>2</sub>).

The ESEM analysis of TiO<sub>2</sub> film prepared from TIP hydrolysis showed no grains at the surface of the film, even at a magnification of 100,000. Therefore, the grains on the surface of the composite films should be composed of nanopowders TiO<sub>2</sub> particles coagulated together by attraction forces and also in the presence of crystallites formed from the alkoxide sol, which could also act as a binder for the particles in the agglomerates.

It was found that the average size of the grains in TiO<sub>2</sub> films prepared by ANP and MPC500 in the sol was approximately 19 and 65 nm, respectively, using Scion Image software (Table 2). The grain size of composite films prepared with ANP is 19 nm is only a little larger than the average crystal size of ANP particles (15 nm), which demonstrates that ANP particles in the sol under these conditions cannot form much larger grains. The grain size of composite film prepared by MPC500 particles in the sol is much larger than the average crystal size of MPC500 particles (5–10 nm), which demonstrates that MPC500 particles in the sol can aggregate to form larger grains.

The normal loads which caused the complete coating removal for sol-gel derived composite films within the scratch track (observed by optical microscope) are shown in Table 2. For sol-gel derived composite films with ANP and MPC500 without heat treatment, normal load needed to remove the films from the substrate was in the range of 8–10 g/mm<sup>2</sup>. The load required for the complete removal

of the composite films increases considerably due to the calcination treatment (Table 2). It is worth mentioning that the composite film with MPC500 had more scratch adhesion than other one, which was confirmed by XRD and SEM images.

### 3.3. Photocatalytic activity

The loss in absorption at  $\lambda_{\max}$  of MO (270 nm and 505 nm) was followed during the photodegradation reaction as a function of irradiation time. The color of MO solution changes from orange and red (in various pH) to colorless with increasing irradiation time, which indicates that there must be some chemical reaction occurring. Control tests showed that adsorption of MO in the reactor vessel was negligible and that a small amount of MO was degraded by photolysis (absence of TiO<sub>2</sub> films) from the lower wavelength UV radiation. The apparent rate constant and degradation rate of ANPSGF-MC are greater than those of MPC500SGF-MC, while the apparent rate constant and degradation rate of MPC500 in suspension is greater than those of ANP. Characterization results of SEM and XRD spectra can explain the enhancement in photocatalytic activity. Firstly, SEM results show that the particle size in ANPSGF-MC is smaller than MPC500SGF-MC. Therefore, ANPSGF-MC possesses a larger surface area. Under the experimental conditions used, the photocatalytic curves follow first-order reaction kinetics. Generally, the photodegradation rates of chemical compounds on semiconductor surfaces follow the Langmuir-Hinshelwood (L-H) kinetics model [15–17].

$$R = \frac{dC}{dt} = k_r \theta = \frac{k_r K C}{1 + K C} \quad (1)$$

where  $k_r$  is the reaction rate constant,  $K$  is the adsorption coefficient of the reactant, and  $C$  is the reactant concentration. The reaction rate  $R$  is proportional to the surface coverage  $\theta$ ; hence a high coverage  $\theta$  or a large adsorption constant  $K$  would result in a high photocatalytic activity. Secondly, XRD measurements further confirm that the crystallite size of ANPSGF-MC is smaller than that of MPC500SGF-MC. All these factors can enhance the photocatalytic activity of ANPSGF-MC.

### 3.4. Factors affecting color removal

#### 3.4.1. Effect of time

The degradation ratios of MO at time intervals of 30 min were studied within 120 min. As shown in Fig. 5, the degradation is increased gradually and almost complete degradation was achieved at 120 min in the presence of ANPSGF-MC, but lower degradation in the presence of

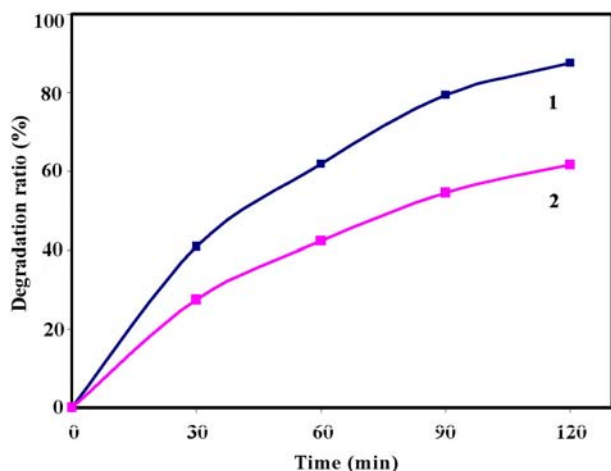


Fig. 5. Effect of irradiation time on photodegradation of 5 ppm MO solution. 1, ANPSGF-MC film; 2, MPC500SGF-MC film.

MPC500SGF-MC was observed (61.7%) at the same condition.

To compare the photocatalytic degradation of composite  $\text{TiO}_2$  films with nanopowder slurries, the dye solution was also photolyzed in the presence of suspensions (dispersions) of ANP and MPC500 at the same weight as films (0.0030 g). The photocatalytic activity order of the suspension catalysts was: MPC500 > ANP and the degradation of MO in the presence of MPC500 and ANP were 96.7% and 45.2% at 30 min, respectively. These results indicate that the degradation in the presence of MPC500 in aqueous suspension is higher than the composite film. The lower photocatalytic activity of ANP suspension is due to larger particle size (15 nm) of the powder and lower surface area ( $\text{m}^2/\text{g}$ ) compared to MPC500.

The composite film prepared by MPC500 showed lower photocatalytic activity than the film prepared by ANP. The impact of surface area on the photocatalytic activity is clearly demonstrated where the MPC500 film shows significantly lower degradation rate than ANP.

Regardless of the sintering mechanism in the presence of the sol-gel-derived binding agents, heating the particulate species at elevated temperatures causes an increase in the contact surface between the neighbor particles, through the neck formation. According to the measured increase in the material's mechanical strength (scratch adhesion), and the form of the grain boundaries (Figs. 4b and c), it is plausible that more sintering in the sol-gel derived composite film with MPC500 occurs during high temperature treatment than ANP. This is in accordance with the change (decrease) in the surface area of this composite film, probably due to smaller particle size and effect of MC as a sintering agent. However, the specific surface area of most of the composite samples, at the heat

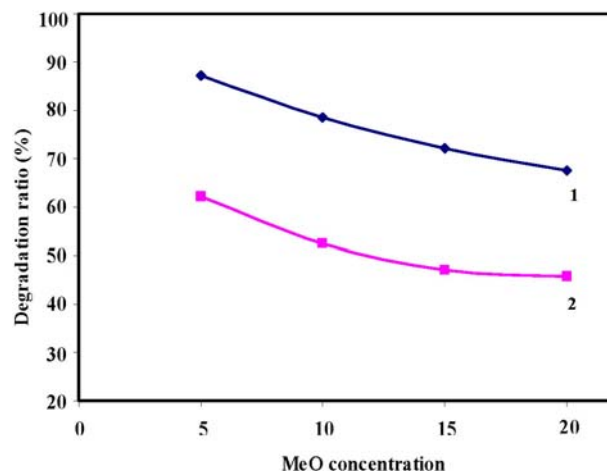


Fig. 6. Effect of initial dye concentration on photodegradation of MO after 120 min of illumination. (1) ANPSGF-MC film; (2) MPC500SGF-MC film.

treatment ( $500^\circ\text{C}$ ), changes mostly due to the increase in the surface area of the sol-gel-derived  $\text{TiO}_2$  (titania sol), as a result the decomposition and oxidation of the organic residues (i.e. MC), the evaporation of the solvent and excess water, etc.

#### 3.4.2. Effect of initial MO concentration

The spectrum of MO in visible region exhibits a main band with a maximum at 505 nm (pH=3.7) and another peak at 270 nm which is due to  $\Pi$  to  $\Pi^*$  transition of aromatic rings of dye. These absorption peaks were diminished and finally disappeared under the photocatalytic conditions.

The effect of initial concentration of MO in aqueous solution on UV photocatalytic degradation rate was investigated over the concentration ranges of 5–20 ppm with ANP and MPC500 films, and the experimental results are shown in Fig. 6, where the degradation rate is decreased with increasing initial concentration of the dye.

Almost complete decolorization of the dye solution was observed (87.2%) after 120 min of illumination using the ANP film at an initial dye concentration of 5 mg/L. At an initial concentration of 20 mg/L, the decolorization was 67.5% at the same time, which is due to fewer photo-generated holes or OH radicals on the catalyst surface because the active sites are covered by dye ions. At a high dye concentration, a significant amount of UV is absorbed by the dye molecules rather than the composite film, which reduces the efficiency of the catalytic reaction [18–20]. As the initial concentration of the dye increases, the requirement of catalyst surface for the degradation is increased [21].

In Eq. (1) when  $C$  is very small, the  $KC$  product is negligible with respect to unity so that Eq. (1) describes

first-order kinetics. The interaction of Eq. (1) with the limit condition that at the start of irradiation,  $t = 0$ , the concentration is the initial one,  $C = C_0$ , which gives

$$\ln(C/C_0) = -kt \quad (2)$$

where  $k$  is the apparent first-order reaction constant. Kinetic parameters resulting from Eq. (2) are reported in Table 3 for different dye concentrations at pH=3.7 using the ANP composite film and pH=2.7 for the MPC500 film. The observed results in Table 3 reveal that the initial dye concentration influences the rate of degradation of the dye.

### 3.4.3. Effect of pH

The photodegradations of MO solutions in the presence of ANP and MPC500 films were studied in the pH range of 2.0–9.0, and the results are shown in Fig. 7. It can be observed that the degradation ratios of MO in the presence of ANP and MPC500 films decrease sharply from pH=2.0 to 9.0. The remarkable photocatalytic degradation ratios of MO in the presence of the composite films indicate that the treatments of some organic pollutants like MO should be performed under acidic conditions. How the pH values affect the photocatalytic degradation of the organic pollutants in the presence of  $\text{TiO}_2$  catalyst is variable and controversial [22]. In general, it is expected that the degradation rate for most organic compounds increases with decreasing pH value, which indicates the number of  $\cdot\text{OH}$  radical increases on the surface of  $\text{TiO}_2$  films in solution by trapping photons [23]. In this case, the highest degradation ratio was also achieved in high acidic solution. At low pH values, the surface of  $\text{TiO}_2$  particles is

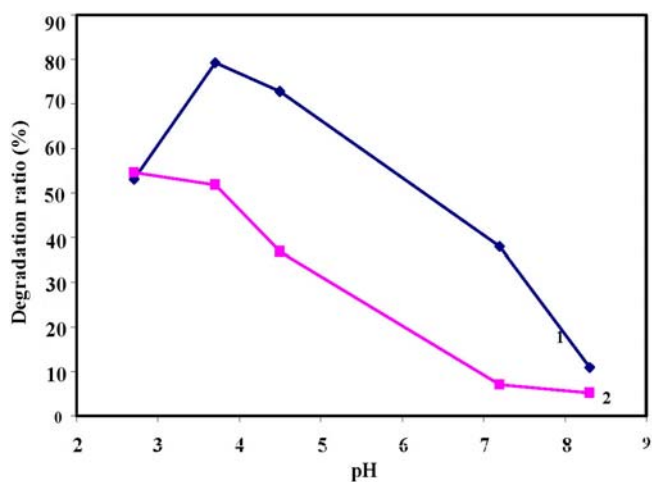


Fig. 7. Effect of pH on photodegradation of 5 ppm MO solution after 120 min illumination. 1, ANPSGF-MC film; 2, MPC500SGF-MC film.

positively charged and is easily capable of adsorbing the MO ion having a negative charge. However, at very low pH values (<3), much adsorption of the dye on the ANP causes a drop in its photoefficiency. It can be explained that at very low pH values the dye was absorbed more strongly and irreversibly on the surface of the composite film and blocked the active sites on the surface of the composite film. At higher pH values, on the surface of  $\text{TiO}_2$  films there are superfluous negative charges which will lead to repulsion to the MO anion in solution, resulting in negligible adsorption.

In suspension systems due to a high ratio of illuminated surface of catalyst and the maximum diffusional distance is very small and almost no mass transfer limitation exists, while in immobilized systems, the accessibility of the catalytic surface to the photons and the reactants and significant influence of external mass transfer, particularly at low fluid flow rate, due to the increasing diffusional length of reactant from the bulk solution to the catalyst surface and the photoefficiency of the immobilized systems is decreased. Therefore, the low photoefficiency of sol-gel derived composite films at pH values above the isoelectric point of  $\text{TiO}_2$  (approximately 5.2 [24]) is reasonable. In addition, the molecular conformation of MO would change the quinonoid form which is unstable and easily destroyed under pH=3.2 (Table 4).

Table 3  
Effect of dye concentration on photodegradation rate of MO

Dye concentration (ppm)	ANPSGF-MC (pH=3.7)	MPC500SGF-MC (pH=2.6)
Rate constant ( $\text{min}^{-1}$ )		
5	0.0172	0.0086
10	0.0128	0.0062
15	0.0104	0.0053
20	0.0091	0.0043

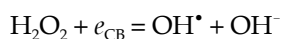
Table 4  
Effect of pH on degradation rate of MO

pH	ANPSGF-MC	MPC500-MC
Rate constant ( $\text{min}^{-1}$ )		
2.6	0.0144	0.0086
3.7	0.0172	0.0080
4.5	0.0083	0.0051
7.2	0.0053	0.0008
8.2	0.0013	0.0005

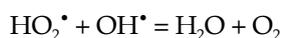
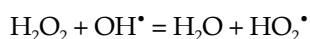
Dye concentration, 5ppm, film thickness,  $\sim 2 \mu\text{m}$ .

### 3.4.4. Effect of hydrogen peroxide

Fig. 8 shows the results of the  $H_2O_2$  effect on the photocatalytic degradation of MO using ANP and MPC500 films. The optimum photocatalytic degradation was observed using 0.2 ml of 30%  $H_2O_2$ .  $H_2O_2$  can capture photogenerated electrons according to the following:



At the same time,  $H_2O_2$  consumes  $OH^\bullet$ :



The effect of added  $H_2O_2$  on the photocatalytic degradation is two-sided. Dionysiou et al. [25] reported that there is an optimum concentration of  $H_2O_2$ . They drew a conclusion that  $H_2O_2$  addition resulted in an increase of the reaction rates with a corresponding increase in photonic efficiency. In high concentration,  $H_2O_2$  either did not enhance or caused a significant inhibition of the mineralization rates.

Furthermore,  $H_2O_2$  can be adsorbed onto semiconductor particles to modify their surfaces and subsequently decrease its catalytic activity [26]. Therefore, the proper amount of hydrogen peroxide could accelerate the photodegradation of azo dye.

### 3.4.5. Repeatability and perspectives

One of the disadvantages for the application of catalysts to decompose organic contaminants is catalyst deactivation due to the strong adsorption of intermediates or carbon species on the catalyst surface. In this case the deactivation catalysts can be regenerated by burning out the chemisorbed carbon species in the air at relatively high temperatures [27].

The repeatability of our composite films was investigated for their potential use in practical systems. Thus, the same composite films washed out and heated at  $100^\circ C$  was used in five consecutive irradiation experiments (cycles) of new added pollutant substrate and the results are presented in Fig. 9. The obtained results make further work on the subject very encouraging, in which there is no need for regeneration at high temperature. In fact, such a simple deposition technique permits the nanopowder  $TiO_2$  incorporation onto the titania film and presents the advantage of significant reduction in the composite catalyst preparation costs and efficiency. In addition, this work opens the possibility of developing more efficient photocatalysts in the form of porous and high surface area inorganic oxide matrixes by depositing photosensitizers (i.e. porphyrines and phthalocyanines). In this direction,

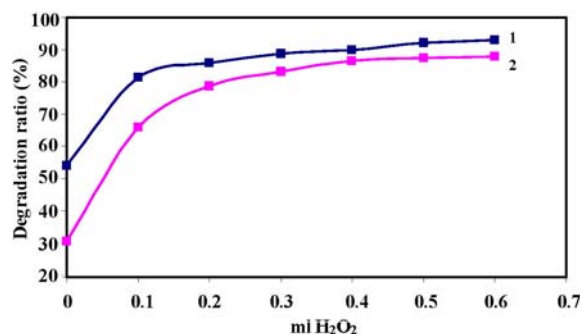


Fig. 8. Effect of  $H_2O_2$  concentration on photodegradation of 5 ppm MO solution after 30 min of illumination. 1 ANPSGF-MC film (pH=3.7), 2 MPC500SGF-MC film (pH=2.6).

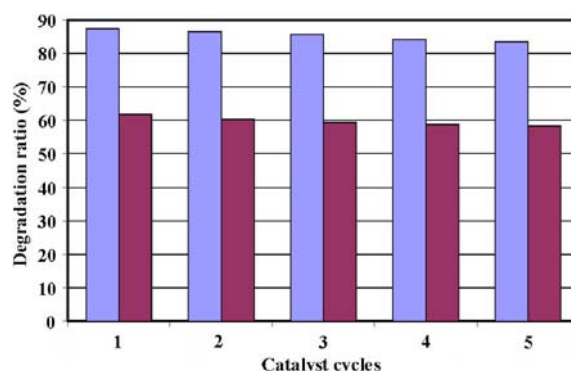


Fig. 9. Effect of reusability of composite films on photodegradation of 5 ppm MO solution after 30 min of illumination. (■) ANPSGF-MC film (pH=3.7); (■) MPC500SGF-MC film (pH=2.6).

the use of  $TiO_2$  precursors with long-range particle size distribution may produce films with high surface development and increased efficiency in light harvesting.

## 4. Conclusions

The nanostructure composite  $TiO_2$  films with good structural integrity and photocatalytic efficiency were fabricated through the sol-gel processing with two commercial titania brands: nanopowder  $TiO_2$  (ANP) and Millennium PC-500 (MPC500). MC was used as a template material for stress reduction during drying.

The MO solution was degraded by the photocatalytic reaction in the presence of nanostructure composite films. The ANP showed that the photocatalytic activity of the composite film is higher than that of the MPC500 while photocatalytic activity of ANP in suspension is less than MPC500. The optimum degradation conditions of MO solution were determined.

The major findings of this study are presented below:

1. Adding MC as a template and low-cost material for stress reduction during drying in the sol not only

improves the amount of crystalline material immobilized on the support, but also the nanosize of the films calcined at 500°C.

2. The results on photocatalytic degradation of MO showed that the increase in photocatalytic activity for ANP calcined at 500°C compared with that of MPC500. Therefore, ANP is a promising nanopowder for the preparation of composite film in applications for the treatment of water.

### Acknowledgment

The authors wish to thank the University of Isfahan for financially supporting this work. We wish to thank Islamic Azad University, Najafabad Branch, for their partial support.

### References

- [1] Z. Wang, U. Helmersson and P.-O. Kall, *Thin Solid Films*, 405 (2002) 50.
- [2] Y. Takahashi and Y. Matsuoka, *J. Mater. Sci.*, 23 (1988) 2259.
- [3] K. Kato, A. Tsuzuki, Y. Torii, H. Taoda, T. Kato and Y. Butsugan, *J. Mat. Sci.*, 30 (1995) 837.
- [4] E. Fredriksson and J.-O. Carlsson, *Surf. Coat. Technol.*, 73 (1995) 160.
- [5] R.W. Matthews, *J. Phys. Chem.*, 91 (1987) 3328.
- [6] R.W. Matthews, *J. Chem. Soc., Faraday Trans.*, 185(6) (1989) 1291–1302.
- [7] L.C. Klein, Processing of nanostructured sol–gel materials, in: A.S. Edelstein and R.C. Cammarata, eds., *Nanomaterials: Synthesis, Properties, and Applications*, Institute of Physics Publishing, Bristol and Philadelphia, 1996, pp. 147–164.
- [8] L.C. Klein, (ed.), *Sol Gel Technology for Thin Films, Fibers, Preforms, Electronics, and Specialty Shapes*, Noyes, NJ, 1988.
- [9] C.J. Brinker, A.J. Hurd, P.R. Schunk, G.C. Frye and C.S. Ashley, *J. Non-Cryst. Solids*, 147–148 (1992) 424.
- [10] D.A. Barrow, T.E. Petroff and M. Sayer, *Surf. Coat. Technol.*, 76–77 (1995) 113.
- [11] M.H. Habibi and M. Nasr-Esfahani, *Dyes Pigments*, 75 (2007) 714–722.
- [12] R.A. Spurr and H. Myers, *Anal. Chem.*, 29(5) (1957) 760–762.
- [13] M. Keshmiri, T. Mohseni and T. Troczynski, *Appl. Catal. B: Environ.* 53 (2004) 209.
- [14] T. Sauer, G.C. Neto, H.J. Jose, R.F.P.M. Moreira, *J. Photochem. Photobiol. A: Chem.*, 149 (2002) 147.
- [15] M.R. Hoffmann, S.T. Martin, W. Choi and D.W. Bahnemann, *Chem. Rev.*, 95 (1995) 69.
- [16] A. Fujishima, T.N. Rao and D.A. Tryk, *J. Photochem. Photobiol., C1* (2000) 1.
- [17] H. Al-Ekabi and N. Serpone, *J. Phys. Chem.*, 92 (1988) 5726.
- [18] C. Zhu, L. Wang, L. Kong, X. Yang, S. Zheng, F. Chen, F. Maizhi and H. Zong, *Chemosphere*, 41 (2000) 303.
- [19] G.A. Epling and C. Lin, *Chemosphere*, 46 (2002) 561.
- [20] I.K. Konstantinou and T.A. Albanis, *Appl. Catalysis B Environ.*, 49 (2004) 1.
- [21] C. Guillard, H. Lachheb, A. Houas, M. Ksibi, E. Elaloui and J.M. Hermann, *J. Photochem. Photobiol. A: Chem.*, 158 (2003) 27.
- [22] D. Bahnemann, D. Bockelmann and R. Goslich, *Solar Energy Mater.*, 24 (1991) 564.
- [23] J.C. D'Oliveira, G. Al-Sayyed and P. Pichat, *Environ. Sci. Technol.*, 24 (1990) 990.
- [24] I. Mazzarino, P. Piccinini and L. Spinelli, *Catal. Today*, 48 (1999) 315.
- [25] D.D. Dionysiou, M.T. Suidan, E. Bekou and I. Baudin, *Appl. Catal. B*, 26 (2000) 153.
- [26] S. Malato, J. Blanco, C. Richter, B. Braun and M.I. Maldonado, *Appl. Catalysis B Environ.*, 17 (1998) 347.
- [27] A. Santos, P. Yustos, S. Rodriguez and F. Garcia-Ochoa, *Appl. Catal. A: Environ.*, 39 (2002) 97.